Results in Physics 7 (2017) 1412–1421

Contents lists available at ScienceDirect

Results in Physics

journal homepage: www.journals.elsevier.com/results-in-physics

Enhanced mechanical behaviors of gradient nano-grained austenite stainless steel by means of ultrasonic impact treatment ☆

Xinjun Yang [a], Xinyue Wang [b], Xiang Ling [c,*], Dongxiang Wang [a]

[a] Jiangsu Key Laboratory of Advanced Food Manufacturing Equipment & Technology, School of Mechanical Engineering, Jiangnan University, Wuxi 214122, Jiangsu, China
[b] School of Electrical Engineering and Automation, Nanjing Normal University, Nanjing 210042, Jiangsu, China
[c] Jiangsu Key Laboratory of Process Enhancement and New Energy Equipment Technology, School of Mechanical and Power Engineering, Nanjing Tech University, Nanjing 211816, Jiangsu, China

ARTICLE INFO

Article history:
Received 19 January 2017
Received in revised form 3 April 2017
Accepted 4 April 2017
Available online 10 April 2017

Keywords:
GNG structure
Mechanical behaviors
Small punch test
Ultrasonic impact treatment
Austenite stainless steel

ABSTRACT

The gradient nano-grained (GNG) structure was formed on the top layer of AISI 304 in the presence of coarse grains (CG) by means of ultrasonic impact treatment (UIT). The impact velocity was 5 m/s and the coverage changed from 3000% to 9000% in order to obtain the microstructure GNG/CG materials. The tensile test and small punch test (SPT) were further carried out in order to investigate the mechanical behaviors of the GNG/CG 304 at the different stress states. The results indicated that the yield strength of GNG/CG 304 obtained by tensile test and SPT increased at the small expense of ductility. The stress triaxiality T played an important role in the deformation behavior of GNG/CG 304. An increased T-value in the region of biaxial stretching of small punch specimen ($T = 2/3$) led to an improved ductility compared with that noted in the case of uniaxial tensile specimen. The strain rate sensitivity m of GNG/CG 304 was 0.0468 that was estimated to be 25-fold greater than the coarse material. The yield strength of GNG/CG 304 at 400 °C was 1.6-fold greater than the coarse material at ambient temperature due to the thermal stability of the GNG layer. Thus, the GNG structure could improve the comprehensive mechanical performances of AISI 304 with a balance of strength and ductility.

Introduction

The 300 series austenitic stainless steels are extensively used in the chemical and food industries, due to their excellent corrosion resistance and favorable formability over a wide temperature range [1]. However, their low mechanical strength and poor antifriction properties restrict them from engineering applications with higher requirements [2]. In addition, the austenitic stainless steel cannot be strengthened by heat treatment due to the specialized microstructure of the material. Thus, grain refinement has been considered to strengthen this type of materials, according to the famous Hall-Petch (H-P) relationship [3].

Nanocrystalline (NC) materials, which are structurally characterized by nanometer-sized grains with a large number of grain boundaries, have been found to exhibit novel properties compared with their coarse-grained counterparts [4]. Nevertheless, the research and development of bulk NC materials are hindered, to some extent, by various difficulties encountered in the synthetic methods used for these materials. Gleiter et al. demonstrated in the early 1980s the first study of preparing bulk NC metals by means of gas condensation and consolidation. Since then, several processing techniques have been developed to produce bulk NC materials [5–7]. However, the preparation of 'ideal' bulk NC samples, free of contamination and porosity, is still a challenge to material scientists, due to the limitation of the aforementioned techniques. As a result most of the current techniques for synthesizing bulk NC materials are not adapted to production on an industrial scale, due to limitations in terms of sample size and cost [8]. Furthermore, extensive investigations over the past few decades indicate that the strength of polycrystalline metals is greatly increased at the expense of their ductility in the presence of a substantial reduction of grain sizes into the nanometer regime [9,10].

In practice, the majority of material failures, such as wear, fatigue, corrosion, originate from surfaces that are sensitive to surface microstructures and properties. The improvement of the surface properties can greatly improve the overall mechanical behavior of the materials [11]. The significance of the surface structure and the attractive properties afforded by the nano-structured materials have led to the development of a new concept namely,

☆ Parts of this paper were presented at the ASME 2014 Pressure Vessels and Piping Conference (Paper No. PVP2014-28239).

* Corresponding author.
E-mail address: Xling@njut.edu.cn (X. Ling).

http://dx.doi.org/10.1016/j.rinp.2017.04.002
2211-3797/

surface nanocrystallization (SNC) [12]. The surface severe plastic deformation (SSPD) method has been considered to be an effective approach to induce SNC [13]. Gradient nano-grained (GNG) structure is formed on the top layer of metals with coarse grains (CG) (GNG/CG structure) by the gradient plastic strain in the absence of a change in the chemical composition (Fig. 1) [14].

Various techniques based on the SSPD method have been successfully applied in the achievement of the SNC in 300 series austenitic stainless steels, and the grain refinement mechanism has been well investigated [15–18]. The following parameters have been investigated by previous studies: tensile strength, thermal stability, fatigue limit of 316L processed by SMAT (surface mechanical attrition treatment) [19–21], stress corrosion crack of 304 processed by SMAT [22], tensile strength of 304 processed by SMAT and UNSM (ultrasonic nano-crystal surface modification) [23–26], tensile strength and corrosion resistance of 304 processed by LSP (laser shock peening) [27,28], wear resistance of 321 processed by SMAT [29], corrosion behavior of 321 processed by UIT (ultrasonic impact treatment) and SP (shot peening) [30,31], corrosion behavior of 316L processed by FMRR (fast multiple rotation rolling) [32] and fatigue behaviors and thermal stability of 304 proccessed by DR (deep rolling) [33]. The results revealed that the tensile strength, fatigue, wear and corrosion properties are improved, although limited information is available on the mechanical behaviors regarding different stress states, strain rates and temperatures of the GNG/CG austenite stainless steel materials.

In the present study, the GNG layers with different microstructures were prepared on the surfaces of the 304 austenitic stainless steels by ultrasonic impact treatment (UIT). It has been reported that UIT demonstrates favorable efficiency with regard to the strain induced grain refinement in stainless steel [16,30,34]. It is flexible and exhibits low cost and excellent controllability that is suitable for industrial applications. The uniaxial and biaxial tensile mechanical behaviors and the dynamic and elevated temperature mechanical behaviors of the GNG/CG 304 were experimentally investigated. The influence of the GNG structure on the mechanical behavior of the GNG/CG 304 material was further explored.

Experimental procedures

Material

AISI 304 was used in the experiments as a typical 300 series austenitic stainless steel, with a composition (wt pct) of 0.058 C, 0.35 Si, 1.32 M, 0.032 P, 0.007 S, 17.45 Cr, 8.28 Ni, balance Fe. The initial grain size was approximately 30 μm and was observed microscopically.

UIT process

The UIT equipment has an ultrasonic generator with a frequency of approximately 21 kHz and an output power of approximately 1.5 kW. The equipment further contains a piezo-ceramic transducer, a step-like ultrasonic horn made from strength material, and the impact head that is installed on the horn tip. The impact head contains cylindrical pin(s) that can freely move between the horn tip and the treated surface. The schematic diagram of UIT is shown in Fig. 2. The mechanical energy P per impact [35] can be estimated considering that pins acquire their kinetic energy from the vibrating ultrasonic horn tip (E_{us}) and from the movement of the impact head/sample (E_r). Thus, it is estimated according to the following expression:

$$P(W/g/impact) = \frac{f_i E_k}{m} = \frac{f_i}{m}(E_{us} + E_r) \approx \frac{f_i}{m}\left[2\pi^2 f_{us}^2 \xi^2 m_p + E_r\right] \quad (1)$$

where $f_i \approx 3 \pm 0.5$ kHz is an impacting frequency and m is the coefficient of the mass dimension. The parameter m includes the correlation between the pin mass m_p and the specimen mass m_s. In the present study, 5 m/s was chosen as the impact velocity. The specimens were divided into five groups and were numbered from 1 to 5 with different coverage. Their coverages were 3000%, 6000%, 9000%, 12,000% and 15,000% according to their corresponding treatment durations namely, 1, 2, 3, 4 and 5 min. The coverage is defined by the following equation:

$$\text{Coverage} = \frac{\text{UIT time (min)} \times 60}{\text{Time required for 100\% coverage of projected are (s)}} \quad (2)$$

Characterization instruments

Microstructural developments along the sections perpendicular to the treated surfaces of the samples were examined by the ZEISS Axio Observer A1m optical microscope. Silicon carbide papers of grade 2000 were employed to mechanically polish cross-sections. Subsequently, the sections were placed on a polishing cloth with a liquid suspension of 0.04 μm alumina, and finally etched in a solution of 25 ml of HNO_3 and 75 ml of HCl at room temperature. The X-ray diffraction (XRD) analysis of the treated specimen was carried out on an X-ray diffractometer (D/max 2500 VL/PC Equipment with CuKα radiation, 6 kW) in the step-scanning mode. A standard SiO_2 specimen was used to calibrate the instrument. Small angular steps of $2\theta = 0.02°$ and a counting time of 2 s were employed to measure the width of the diffraction peak. The Scherrer and Wilson method was also used to estimate average grain size from line broadening of Bragg diffraction peaks.

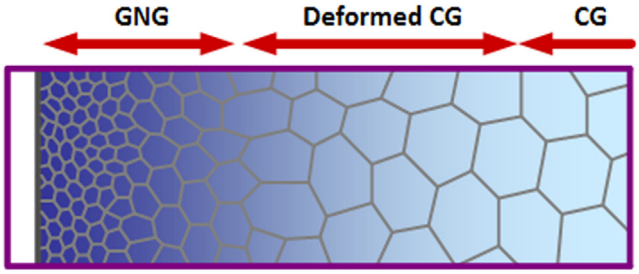

Fig. 1. Schematic of the cross-sectional microstructure of GNG/Deformed CG/CG core [14].

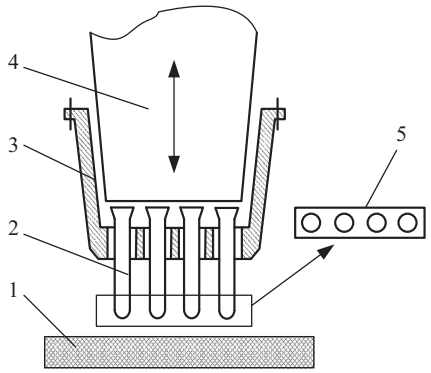

Fig. 2. Impact head in UIT equipment: (1) specimen, (2) pins, (3) pins holding, (4) ultrasonic horn, and (5) the arrange of the pins on the head.

Results and discussion

Microstructures of processed specimens

Fig. 3 and 4 indicate the metallographs of the cross-sections of samples 1, 2, 3, 4 and 5. A total of three typical regions are observed following the treatment when the coverage is set at 9000%: A, gradient nano-grained Layer (white region in the metallograph); B, severe plastic deformation band (black region in the metallograph) and C, small deformation area. NCs in GNG layer have different erosional characteristics for large grain boundaries related to the coarse material, and show different etching pattern. Thus, a clear demarcation exists between regions A and B. The thickness of A is estimated to 170 μm. It should be noted that when the coverage is lower than 9000%, the GNG layer is thin and inhomogeneous. When the coverage reaches 9000%, the GNG layer is homogeneous, and its thickness is notably unchanged.

Fig. 5 illustrates the X-ray diffraction (XRD) patterns for the different treatment coverage, while Fig. 6 illustrates the patterns of sample 3 at the different depths after the treatment. The martensite diffraction peaks appear in all treated samples indicating that high strain and the strain rate caused by UIT induce martensite transformation in the austenite stainless steel. The content of martensite increases as the coverage increases from 15% to 32%, whereas when the coverage reaches 9000%, the content is saturated to a major extent (Fig. 7). According to Ref. [36], strain rate in the range of 10^2–10^3 s^{-1} can produce a very large dislocation density, leading to a large number of nucleation sites for α′-martensite transformation in AISI 304. Nevertheless, the higher strain rate tends to impede α′-martensite transformation due to deformation twinning. The high strain rate induced by UIT (larger than 10^5 s^{-1}) could impede martensite transformation effectively. The martensite and refined grains disappear at the depth of approximately 200 μm that is in agreement with the results shown in Fig. 2. The surface grain size is smaller than 30 nm and further decreases at a minor extent when the coverage reaches 9000% (Fig. 8). The data suggest that the microstructure of the GNG layer is stable with slight variations when the coverage is larger than 9000%. Thus, the coverage range of 3000–9000% was selected as the input parameters of UIT in order to produce GNG/CG 304 stainless steels with different GNG structures.

Mechanical behaviors at uniaxial tensile stress state

The specimens exhibit a dog bone shape with 5 mm thickness and the gauge length is 10 mm (Fig. 9). The tensile strain rate is 10^{-3} s^{-1} and the three specimens were tested to ensure the repeatability of the procedure. Both sides of the specimen were treated by UIT. The tensile stress-strain curves of treated specimens are shown in Fig. 10, and the parameters of mechanical properties are listed in Tables 1 and 2. The results indicate that the 0.2% offset yield strength $\sigma_{0.2}$ has been improved with the decrease in the surface grain size and the increase in the GNG thickness. The latter two parameters were induced with higher coverage. The 0.2% offset yield strength $\sigma_{0.2}$ is enhanced from 306 MPa to 373, 401, and 433 MPa resulting in corresponding enhancements of ~22%, ~31% and ~42%, respectively compared with the untreated specimens. The enhancements refer to samples 1 to 3, respectively. The enhancement noted was lower than the GNG/CG 304 stainless steel samples processed by UNSM and SMAT as regards the thicker specimens in the test with smaller proportion of GNG layer over the complete specimen [23,24]. However, the ultimate tensile strength σ_b was not considerably changed following the treatment. This indicates that the accumulation of damage is not changed during the induction of the GNG layer in 304 and it is not associated with the grain size and thickness of the GNG layer. The elastic modulus of the specimen decreased following UIT processing (inset graphic in Fig. 9). The elastic modulus of GNG/CG 304 is 131.5 GPa with the decrease of ~29% (Table 1). The elastic modulus of GNG/CG metal depends on the residual stress profile and the thickness of the processed specimen [37]. The high compressive residual stress on the top and on the subsurface promotes the plastic deformation at the central region of the specimen under moderate level of loading, whereas the surface region is retained at the elastic stage. The latter processes lead to an "apparent" elastic deformation of the entire specimen. This is attributed to the fact that the central and surface regions have the same amount of strain with the former having plastic deformation and the latter having elastic deformation. This in turn results in a large portion of the load acting on the surface region and the smaller elastic modulus of the GNG/CG 304 compared with the untreated specimen [37,38]. In addition, the reduction of the elastic modulus of GNG/CG 304 is lessened when the treatment coverage increases. This is attributed to the fact that the residual stress is saturated and the residual stress profile is minimally altered irrespective of the extent of the coverage in the UIT condition, during the adjustment of the coverage to 2000%.

In contrast to the aforementioned observations the tensile elongation decreased by 8.3%, 11.0% and 17.6% for the specimens 1–3, respectively, as a result of the decrease of the surface grain size and the increase of the GNG thickness. The engineering strain can be converted to the true strain. Furthermore, the true strain to fracture ε_{total} can be divided into two sub-strains namely, the uniform true strain prior to necking ε_{unif} and the true strain following the onset of necking ε_{neck}. The uniform true strain prior to necking decreases from 0.55 for the untreated specimen to 0.527, 0.516 and 0.484, respectively (Table 2). However, the true strain following the onset of necking is minimally altered in the presence of the processing condition. The strain-hardening coefficient n is obtained by fitting of the true stress-strain curves that reflect the homogeneous strain of the metal hardening capacity and the ductility. The corresponding values of n were 0.48 for the untreated sample and 0.37, 0.37, 0.35 for samples 1–3, respectively. According to Considère's criterion, the strain-hardening coefficient is numerically equal to the uniform true strain provided that a metal follows the Hollomon's relationship [39]. However, the strain-hardening coefficients obtained from the 304 stainless steel, following processing, were lower than the corresponding uniform true strains. This is due to the effect of the strain-rate sensitivity on the uniform true strain of this alloy [39]. Similar trends between strain-hardening coefficients and uniform true strains are noted for the original and processed 304 with different GNG structure. Thus,

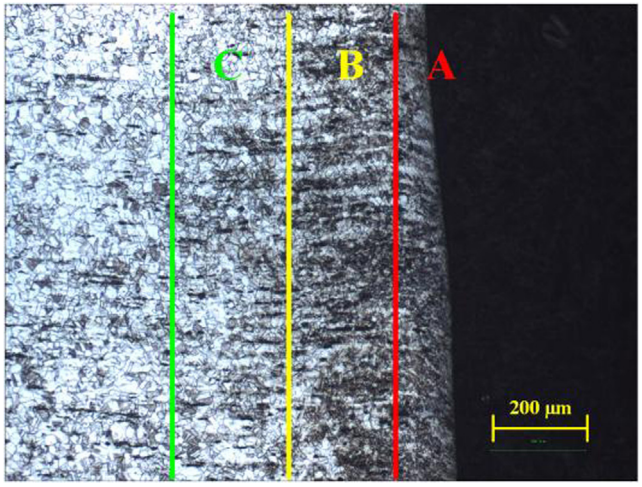

Fig. 3. Section metallograph of sample 1.

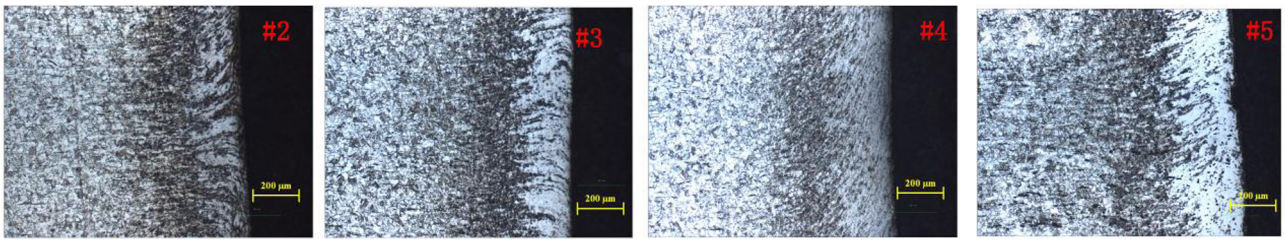

Fig. 4. Section metallographs of sample 2, 3, 4, 5.

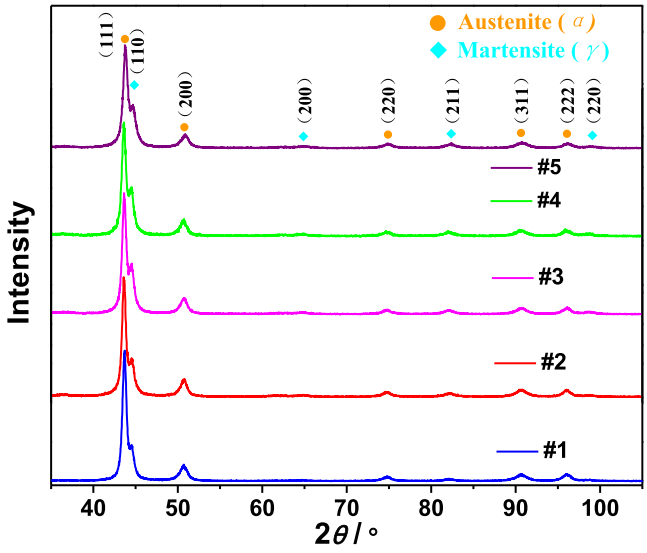

Fig. 5. XRD patterns on the surface treated with different coverage.

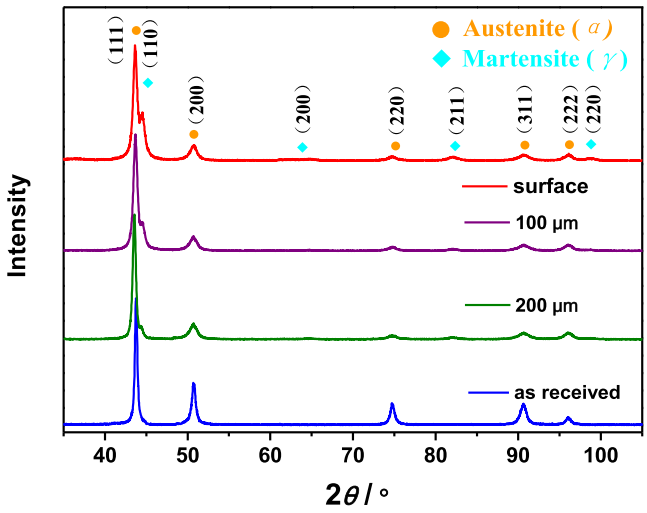

Fig. 6. XRD patterns at different depths of sample 3.

the strain-hardening coefficient can reflect the uniform true strain and the ductility of GNG/CG 304.

The tensile fracture morphology of GNG/CG 304 with the coverage of 3000% is shown in Fig. 11. The fractography presents a typical ductile fracture. Visible boundary forms between the nano-grained layer and the zone full of dimples were noted on the top surface. The size of the dimples was altered from the treated surface to the matrix beneath the nano-grained layer. According to the finite element modeling (FEM) developed by Tian [38], the

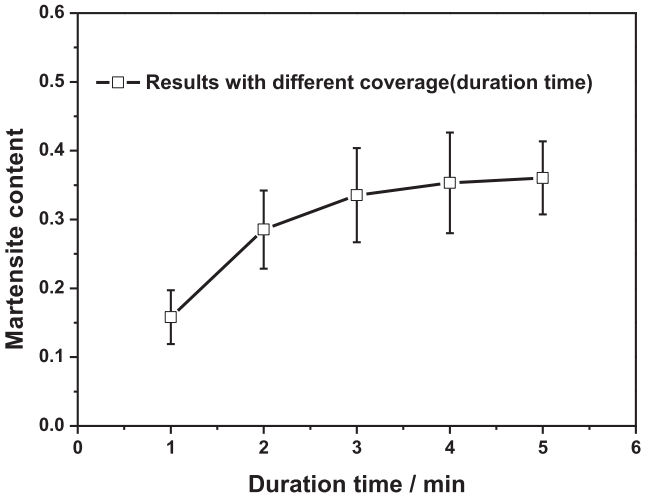

Fig. 7. Volume contents of martensite with different coverage.

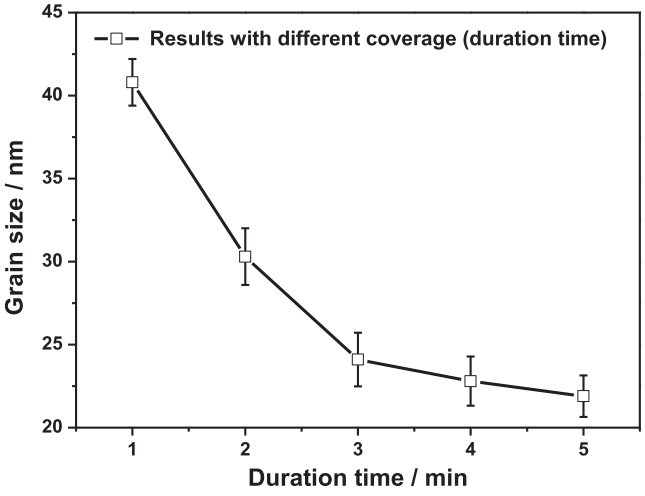

Fig. 8. Surface grain sizes with different coverage.

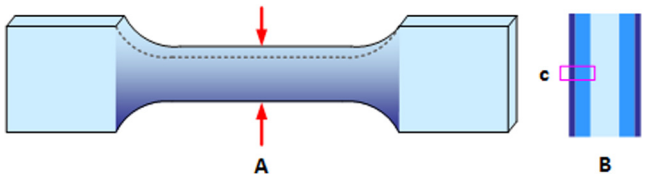

Fig. 9. Schematic of tensile specimen following UIT (B is the cross section of specimen located by A, and the microstructure of part C is shown in Fig. 1).

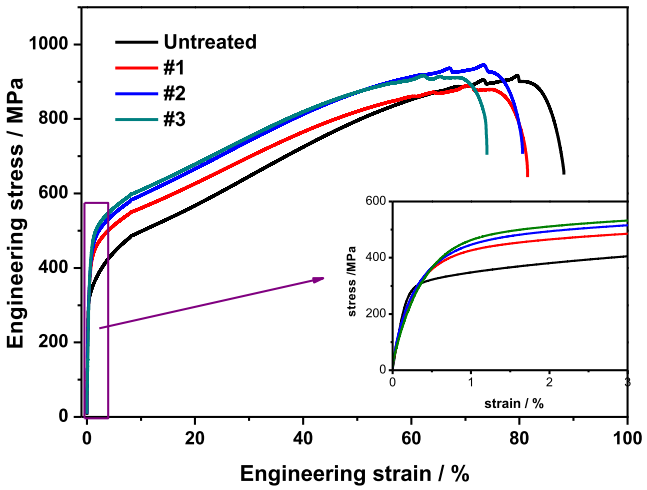

Fig. 10. Stress-strain curves of GNG/CG 304.

GNG/CG structured metal undergoes plastic deformation as regards the gradient hardness and strength induced by the gradient structure. This process occurs during the turn from the central region to the surface. The central region undergoes plastic deformation at the stage of the elastic elongation step of the GNG/CG 304. As a result, the accumulation of the plastic strain and the long deformation time suffice growth and coalesce of the fine cavity in the central region and result in the corresponding fractography that includes a gradient structure.

It can be expected that the strength of GNG/CG 304 is improved at the expense of ductility, possibly due to the nano-grained structure on the surface layer. As regards nano-grained materials, the majority of the dislocation sources are not active, and insufficient dislocation is required to sustain the plastic elongation [40]. In addition, the dislocation cannot be stored inside the tiny grains efficiently due to the nanoscale grain boundaries that act as sinks of dislocation annihilation [41]. The aforementioned processes result in the minimal ductility of the nano-grained materials. In addition, the strength of the GNG/CG 304 stainless steel is improved evidently in the presence of a minimal loss of ductility compared with the nanoscale and coarse materials. The confined GNG layer exhibits a high yield strength and tensile ductility, due to the elasticity and the plastic gradient of the AISI 304 of GNG/CG structure. Furthermore, the strain localization of GNG layer is effectively suppressed by the CG substrate (The grain boundary slip and migration mediate the plastic deformation of GNG layer) that offers the apparent mechanical responses [24]. It has been further reported that the tensile ductility of GNG/CG metals is limited by the CG substrate, and is not associated with the GNG layer [24]. Taken together, the findings indicate that GNG/CG 304 has an improved ductility compared with the aforementioned tensile specimens processed by UNSM and SMAT. Since the tensile specimens investigated in the present study exhibited thicker CG substrates, samples 1 and 2 exhibited the approximate value of the uniform true strain. The 304 specimens processed with coverage of 3000% and 6000% contain very thin GNG layers (Figs. 3 and 4). As a result, the thicknesses of the CG substrates were similar and resulted in the similar ductility for both samples 1 and 2. However, the grain sizes of the GNG layers were different for the two specimens. Consequently, sample 2 that had a smaller grain size on the surface layer exhibited an improved yield strength compared with sample 1.

Table 1
Mechanical properties of different samples-part I.

Sample No.	Yield strength $\sigma_{0.2}$/MPa	Ultimate tensile strength σ_b/MPa	Elastic medule E/GPa	Strain hardening coefficient n
Untreated	306	905	185.3	0.4812
#1	373	890	131.5	0.3705
#2	401	917	122.8	0.3735
#3	433	901	108.5	0.3507

Table 2
Mechanical properties of different samples-part II.

Sample No.	True strain to fracture ε_{total}/%	Uniform true strain before necking ε_{unif} /%	True strain after the onset of necking ε_{neck}/%	Elongation A/%
Untreated	63.3	55.0	8.0	81.2
#1	59.6	52.7	6.9	74.5
#2	58.3	51.6	6.7	72.3
#3	55.4	48.4	7.0	66.9

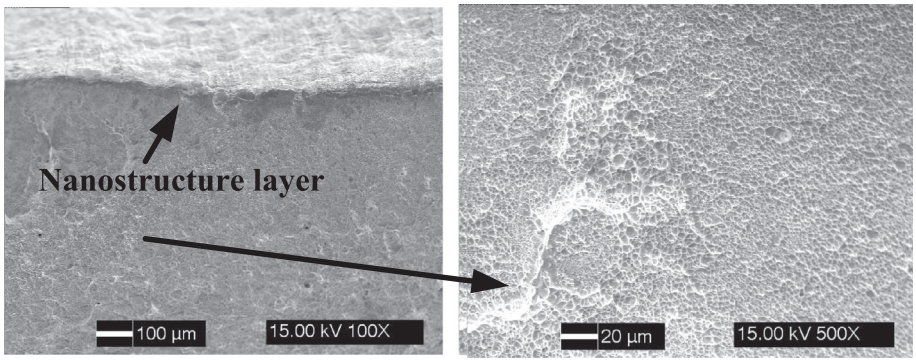

Fig. 11. Fracture morphologies of GNG/CG 304.

Effects of strain rate on the mechanical behaviors of GNG/CG 304

Strain rate has a significant influence on the tensile properties and fatigue lives of the materials under different work conditions [42]. UIT can improve the fatigue life and strength of stainless steel. The reliable design of structural components requires an understanding of the dynamic mechanical properties and the relation between the tensile properties at relevant strain-rates. The strain rate sensitivity m indicated the effect of the stain rate on the metallic material property alterations in grain size from micrometer to nanometer. GNG/CG 304 that is featured by a gradient variation in grain size exhibits different stain rate sensitivities at different depths resulting in a dynamic property. The processed specimens with 3000% coverage were selected for tensile application at the broad strain rates ($10^{-3}\ s^{-1}$, $5\times10^{-3}\ s^{-1}$, $10^{-2}\ s^{-1}$, $5\times10^{-2}\ s^{-1}$) in order to investigate the strain rate sensitivity of GNG/CG 304. The processed specimens were identical with the aforementioned specimens (Section "Mechanical behaviors at uniaxial tensile stress state").

Fig. 12 describes the engineering stress-strain curves versus different strain rates, while the rectangle region of partial curves is enlarged in the graph. The engineering stress and the engineering strain exhibit a linear relationship, while the engineering strain is lower than 0.5%. The strain rate does not demonstrate a considerable effect on the shape of the stress-strain curve, and no significant change is observed in the slope of the linear region regarding the graph of the increase of the strain rate. The elastic module of GNG/CG 304 was not altered with the strain rate, although the stress-strain curve was increased according to the increment of the strain rate. The yield strength increased gradually with an approximate value of 20% at the strain rate of $5\times10^{-2}\ s^{-1}$.

The effect of strain rate on stress-strain curve can be reflected by the Hollomom equation, and the strain rate sensitivity m is defined by following formula:

$$m=\left.\frac{\partial \ln\sigma}{\partial \ln\dot{\varepsilon}}\right|_{\varepsilon} \tag{3}$$

Fig. 13 illustrates the strain rate sensitivity of GNG/CG 304 at different strains. The results indicate that the stain rate sensitivity is approximately invariant at different strain rates, while it declines from 0.051 to a constant value of 0.0468, during the increase in the strain (0.08). The strain rate sensitivity m can further be calculated by the following equation (4) [43]:

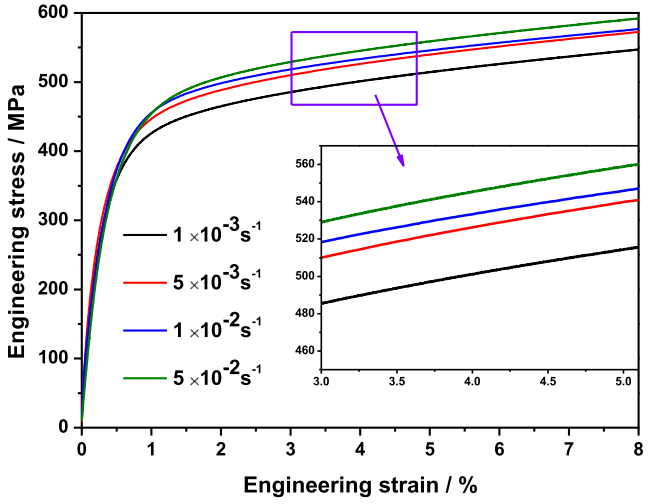

Fig. 12. Strain-stress curves against different strain rates.

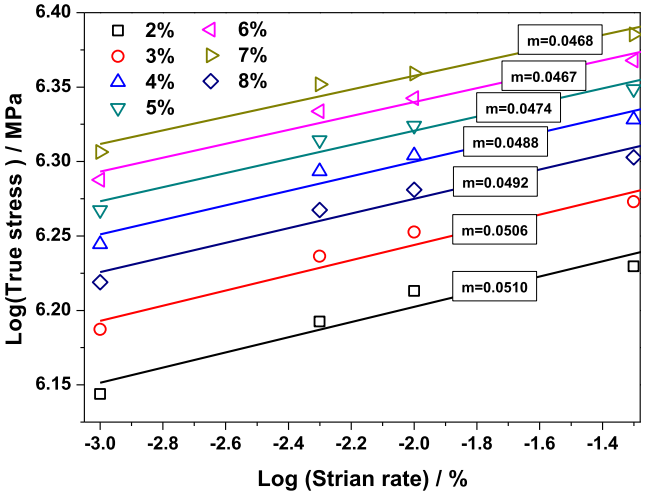

Fig. 13. Stress–strain rate curves at different strains.

$$m=\frac{3^{1/2}kT}{V\sigma_y} \tag{4}$$

where k is the Boltzmann constant, T is the absolute temperature, V is activation volume, and σ_y is flow stress. According to Eq. (3), the strain rate sensitivity m decreases with the increase of flow stress at the early stage of plastic deformation. The high flow stress means high strain resulting in the variation of strain rate sensitivity with the strain presented in Fig. 12.The activation volume of the dislocation processes ranges between the order of 100 to $1000b^3$ (b is magnitude of the Burgers vector) and is related to forest dislocation cutting for fcc metals. The activation volume of the grain boundary (GB) slip or migration mechanism is approximately estimated at the range of $1–10b^3$ [44]. During the grain size decrease, the dislocation slip is suppressed and the GB diffusion (slip and migration) gradually increases. The corresponding V-value for NC fcc metals, exhibiting enhanced rate sensitivity of plastic flow, is found to be reduced by nearly two orders of magnitude [44]. As regards coarse-grained 304, the m value is approximately 0.002, and a relatively weak grain size dependence of m has been reported for the dislocation mechanism [45]. GNG/CG 304 has a significantly higher percentage of GBs in the GNG layer compared to the coarse-grained counterparts. The dislocation slip is suppressed when the GB diffusion gradually increases and mediates the plastic deformation of the GNG layer. This results in the low activation volume. In addition, the dislocation slip inhibited by the high density of coherent twin boundaries in the GNG layer further contributes to the improved strain rate sensitivity. The significantly enhanced strain rate sensitivity m of GNG/CG 304 is increased at a rate greater than 25-fold compared with that for the coarse specimen that indicates that gradient nanostructure surface layer can improve the dynamic mechanical performance of the 300 series stainless steel.

Mechanical behaviors at biaxial tensile stress state

The small punch test (SPT) is used to investigate the mechanical behaviors of GNG/CG 304 in which the load condition is biaxial. The process of the test is illustrated in Fig. 14. The SPT specimen is a small disk with a diameter of 10 mm and a thickness of 0.5 mm (Fig. 15). A total of three specimens are tested to ensure the repeatability. The specimen is clamped in the center of the die, and the load is applied to the specimen from a ball with a punch. Subsequently, the deflection of the specimen center and the applied load are monitored and recorded by transducers during the deformation. The specimens are treated on one side. During the

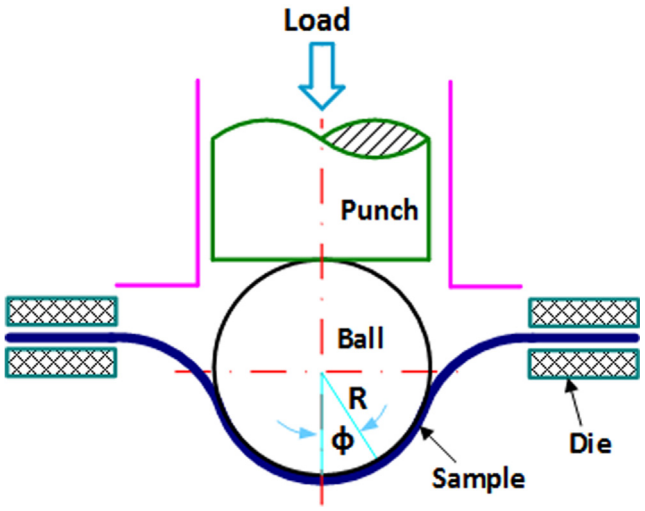

Fig. 14. Schematic diagram of small punch test.

test, the ball comes in contact with the untreated surface, and the load – deflection (L-D) curves are constructed (Fig. 16). Typical stages depicting the behaviors of materials during deformation are marked on the curves. The first stage, elastic bending, is associated with local surface microyielding. During the second stage, plastic bending, plastic flow begins and spreads within the sample-punch contact zone. Biaxial deformation of flat sample into a dome-shaped cap occurs during the next stage, membrane stretching. Once maximum load capacity is reached, unstable plastic flow begins leading to formation of cracks and sample failure (Fig. 17). The yield strength σ_s, tensile strength σ_b and elongation A can be determined by the following three equations:

$$\sigma_s = \alpha(p_y/t_0^2) \tag{5}$$

$$\sigma_s = a(p_m/t_0^2) - b \tag{6}$$

$$A(\%) = \lambda\frac{d_m}{t_0} \tag{7}$$

where P_y is the elastic plastic transition load, P_m is the maximum load, t_0 is the sample thickness and d_m is the maximum displacement of the ball. α, a, b and λ are material parameters, and their values are equal to 0.36, 0.13, 320 and 16.07, respectively for AISI 304 [46].

The results summarized in Table 3 reveal that the yield strength σ_s for the untreated specimen is 300 MPa that is in agreement with the result obtained from the tensile test. Following coverage treatment, different GNG structures are formed on the surface of 304 specimens. The yield strength σ_s is increased gradually and is apparently developed. The maximum value of σ_s is 803 MPa for sample 3, which is estimated to 268% greater compared with the untreated specimen. Considering the different thicknesses

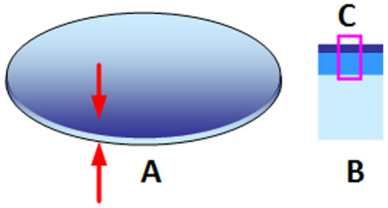

Fig. 15. Schematic of SPT specimen after UIT (B is the cross section of specimen located by A, and the microstructure of part C is shown in Fig. 1).

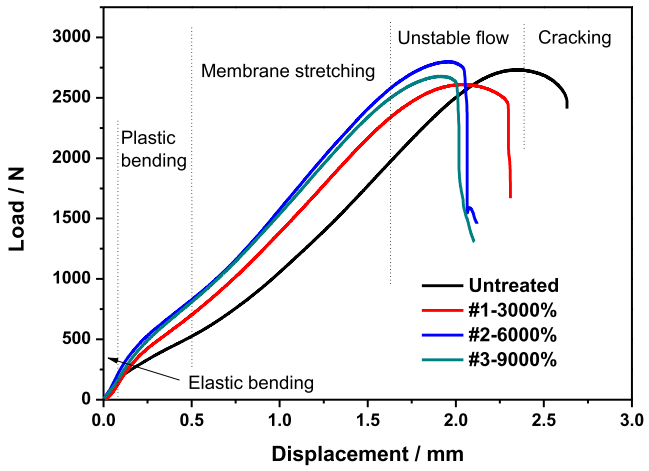

Fig. 16. L-D curves of GNG/CG 304.

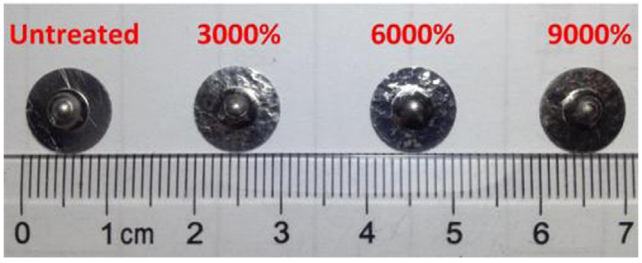

Fig. 17. Specimens of SPT after the tests.

Table 3
Mechanical properties of different specimens in SPT.

Sample No.	Yield strength $\sigma_{0.2}$/MPa	Ultimate tensile strength σ_b/MPa	Elongation A/%
Untreated	302	993	74.9
#1	610	954	66.2
#2	704	1024	61.5
#3	807	966	60.8

between the tensile and SPT specimens, the ROMs of Voigt was employed to compare the yield strength of GNG specimens with different thicknesses [47].

$$\sigma_{GNG/CG} = \frac{\sigma_{GNG} \times h_{GNG} + \sigma_{CG} \times h_{CG}}{h_{total}} \tag{8}$$

where σ_{GNG} is the yield strength of the GNG layer. σ_{CG} is the yield strength of the CG substrate. h_{GNG} and h_{CG} are the thickness parameters of the GNG layer and the CG substrate, respectively. h_{total} is the entire thickness of the GNG/CG specimen and equal to h_{GNG} and h_{CG}. The results indicate that the yield strength of the GNG/CG specimens with thickness of 0.5 mm under biaxial loading is in concordance with that noted due to uniaxial tensile loading with different GNG structures. The ultimate tensile strength σ_b is similar in value prior to and following the treatment. Additionally, it is independent of the thickness of the GNG/CG specimens and approximate to the value of the corresponding specimens gained from the tensile test.

However, the elongation A of the untreated specimen in SPT is lower than that of the tensile specimen that indicates that the equation used is subject to errors in the estimation of the elongation value of the SPT specimens. A linear relationship is reported between the elongation and the maximum displacement. Thus, it

can be estimated that the elongations of GNG/CG 304 decrease by 11.6%, 17.8% and 18.8% respectively, compared with the untreated specimen in SPT. The ductility of the specimens in SPT is slightly lower compared with the tensile specimen. It should be noted that the specimen thickness in SPT is 0.5 mm. The CG substrate is thinner than the tensile specimen. The elongation of the tensile specimen processed by SMAT that exhibited a 1 mm thickness was estimated to 50% of that noted in the untreated specimen [23]. Thus, it is reasonable to conclude that GNG/CG materials exhibit excellent ductility under biaxial loading in comparison with the uniaxial loading. This may be attributed to the stress triaxiality T (a ratio of hydrostatic stress to Mises stress), which plays a significant role in the plastic deformation of ultrafine-grained (UFG) and nano-grained metallic materials. A high value of T can trigger microshear banding and promote the GB migration and slip processes of the UFC and NC materials [48]. The T value increases in the necking region ($T > 1/3$) of the specimen in tensile test, while the value is equal to 1/3 in the homogeneous tensile deformation stage. The increase in the value of T aids GNG/CG 304 materials to sustain similar true strain following the onset of necking ε_{neck} compared with the untreated specimen. In the region of biaxial stretching of small punch specimen, the T value is equal to 2/3 which exceeds the T value in the necking region of the tensile specimen, thus leading to an improved ductility compared with that of the uniaxial tensile specimen. Figs. 18 and 19 are the fractographes of tensile test and SPT samples. Dimples are formed in the surface layer of GNG/CG 304 in SPT (shown by arrow in Fig. 18), instead of smooth fracture presented on surface of GNG/CG 304 in tensile test (showed by arrow in Fig. 19). Better ductility of GNG/CG 304 at biaxial stress state is also proved by the comparison.

Mechanical behaviors at high temperature

GBs in the GNG layer derived from the twin boundaries and dislocation structures possess high excess energies and tend to increase notably at the high temperature that would restrict potential applications. The high temperature SPT is carried out in order to study the high temperature performances of GNG/CG 304. The tests were conducted at the following temperatures: ambient, 200 and 400 °C that represent the universal applicable range of the temperature for AISI 304 (ruling out the effects of creep and sensitization). The test specimens were untreated, whereas 304 and sample 2 were processed with coverage of 6000%. The L-D curves are shown in Fig. 20, and the corresponding results are summarized in Table 4. The elongations obtained by Eq. (7) exhibit limited precision, although they can provide a general guideline regarding the ductility change. The results show that GNG/CG 304 demonstrates an improved performance compared with CG 304 at high temperatures. The relationships among yield strength, elongation and temperature are exhibited in Fig. 21. The yield strength, tensile strength and elongation of both specimens decreased during a temperature rise, and approximately linear relationships between any of the aforementioned parameters and the temperature were presented provided the ultimate tensile strength value of the untreated sample at 200 °C is not considered. The slopes were similar for the specimens prior to and following the UIT. This finding indicates that the associations of ductility and strength with the temperature for the CG 304 and GNG/CG 304 are similar. The latter similarity may be attributed to the stability of the GNG structure at elevated temperatures. The isothermal grain growth can be described by the Eq. (9) [49,50]:

$$D^{1/n} - D_0^{1/n} = k_0 t \exp\left(\frac{-Q}{RT}\right) \tag{9}$$

where D is the grain size at time t, D_0 is the initial grain size, n is the time exponent ($1/n$ is called grain growth exponent), Q is the acti-

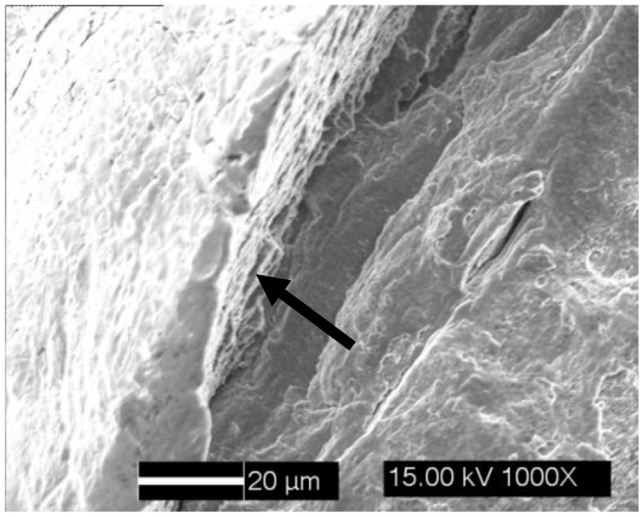

Fig. 19. Surface layer fracture morphologies of SPT sample.

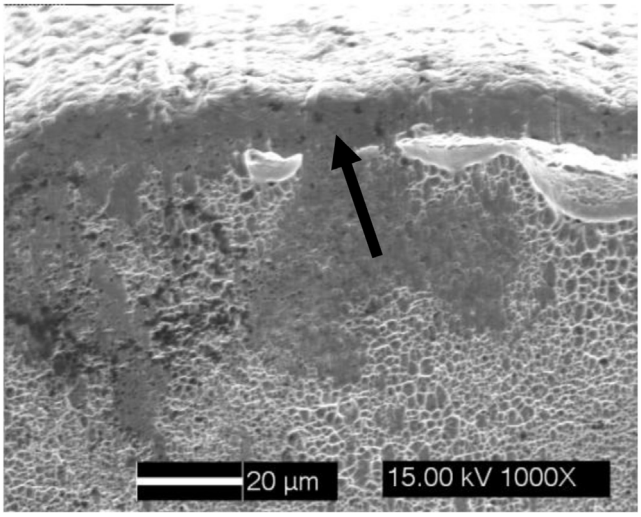

Fig. 18. Surface layer fracture morphologies of tensile test sample.

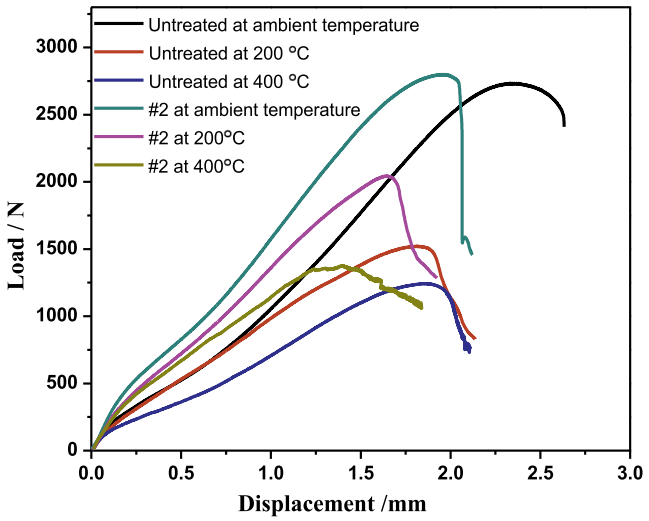

Fig. 20. L-D curves of specimens at different temperatures.

Table 4
Mechanical properties at different temperatures (SPT).

Sample No./ temperature	Yeild strength σ_s/ MPa	Tensile strength σ_y/MPa	Elongation A/%
Untreated/Ambient	302	993	74.9
Untreated/200 °C	256	472	59.5
Untreated/400 °C	195	326	53.0
#2/Ambient	704	1024	62.9
#2/200 °C	561	743	53.0
#2/400 °C	501	397	44.0

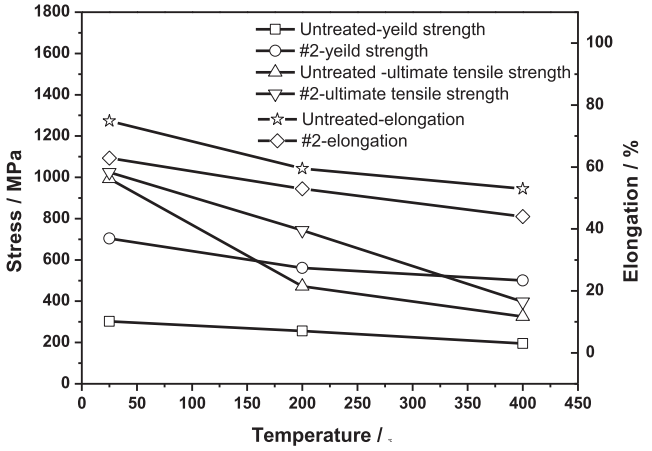

Fig. 21. Relationships between yield strength, ultimate tensile strength, elongation and temperature.

vation energy for grain growth, k_0 is a rate constant that is independent of the absolute temperature T, and R is the molar gas constant. It is important to note that the time exponent n in NC and UFG materials is less than 0.1 in the different alloying systems when $T < T_c$ [49,51] (T_c is the transition temperature, and it is estimated to 600 °C for AISI 304 [52]). The fact that the time exponent n of the NC materials differs to 0.5 (ideal value of n) suggests that grain boundary pinning forces are operative [49] that inhibit the growth of the nano-sized grains. It has been previously suggested that elements such as V, Nb, Ti, and Mo can form complex carbonitrides in the steel matrix [51]. This in turn increases the grain growth activation energy Q and results in Zener pinning effects, due to the contribution of the high grain size stability of the GNG 304 stainless steel. The GNG structure that was generated by deep rolling of 304 was reported to be stable up to 600 °C using an annealing time of 10 min [52]. When the annealing time was extended between 10 and 100 h, the surface grain size was lower than 200 nm. According to the Hall-Petch relationship, the stable grain size of the GNG structure at the elevated temperature retains the GNG/CG 304 behavior compared with the untreated CG 304. The yield strength of GNG/CG 304 and CG 304 decreases to 28.8% and 35.4%, respectively during a temperature rise to 400 °C. The yield strength of GNG/CG 304 was 501 MPa at 400 °C. The latter is 1.6-fold higher compared with the untreated CG 304 at ambient temperature. Although the elongation of GNG/CG 304 decreases to 0.44 at the temperature of 400 °C, it is sufficient for the engineering application. Thus, the GNG structure generated by UIT enhances the high temperature mechanical behaviors of the 304 stainless steel effectively and is potentially useful in the industrial application.

Conclusions

The gradient nano-grained structure was formed on the top layer of AISI 304 with coarse grains by ultrasonic impact treatment. The impact velocity was 5 m/s and the coverage ranged from 3000% to 15,000% in order to obtain the GNG/CG 304 material with different microstructures. The parameters surface grain size, martensite content and GNG layer thickness increased at a proportional ratio with the coverage, although the micro-structure was stable when the coverage reached 9000%. The tensile and small punch tests were further conducted to investigate the uniaxial and biaxial mechanical behaviors of the GNG/CG 304 material that was processed with the coverage of 3000%, 6000% and 9000%. The following conclusions are highlighted:

1) The yield strength of GNG/CG 304 that was obtained in the tensile test and in the SPT folloeed ROMs of Voigt, and it increased according to the decrease of the grain size and the increase of the GNG layer thickness during ductility expansion. However, the GNG/CG 304 and the CG 304 materials exhibited similar ultimate tensile strength values with different specimen thicknesses at both uniaxial and biaxial tensile stress states.
2) The uniform true strain prior to necking ε_{unif} of the tensile specimen decreased from 0.55 to 0.484 with the increasing thickness of the GNG layer, whereas the strain-hardening coefficient n further decreased from 0.48 to 0.35. The fractography presented a typical ductile fracture. The size of the dimples was altered gradually from the treated surface to the matrix. The strain localization of the GNG layer was effectively suppressed by the CG substrate, and the ductility of the GNG/CG 304 material was notably dependent on the thickness of the CG substrate at the uniaxial tensile stress state. The GNG/CG 304 specimens with CG substrates exhibited similar ε_{unif} and n values.
3) The GNG/CG 304 SPT specimen exhibited an improved ductility compared with that noted in the uniaxial tensile specimen, which is attributed to the high stress triaxiality T. A high T-value (2/3 in biaxial stretching of small punch specimen) promotes the GB migration and slip processes of the NC materials. In contrast, the increase of the T-value in the necking region of the tensile specimen ($T > 1/3$), following the onset of necking ε_{neck}, results to a similar true strain parameter of the GNG/CG 304 specimen compared with the coarse specimen.
4) The strain rate sensitivity m of GNG/CG 304 was estimated to 0.0468 and was 25-fold greater compared with the coarse specimen, due to the significantly higher percentage of GBs in the GNG layer. The dislocation slip was suppressed and the GB diffusion gradually increased, thereby causing the plastic deformation of the GNG layer and resulting in a low activation volume and a considerably high m-value. This finding suggested that the GNG surface layer can improve the dynamic mechanical performance of the 304 stainless steel.
5) The ultimate tensile strength of the 304 material at the elevated temperature did not change prior to and following the UIT, although the yield strength was apparently improved by the GNG surface layer. The yield strength of GNG/CG 304 at 400 °C was 2.6-fold greater compared to the coarse specimen at ambient temperature as regards the thermal stability of the GNG layer. The elongation required for the engineering application was not sufficiently achieved despite the decrease in the elongation of GNG/CG 304 to 0.44 at 400 °C.

Acknowledgement

The authors wish to acknowledge the financial support provided by the National Natural Science Foundation of China (Grant

No. 51505189), and Open Project of Jiangsu Key Laboratory of Advanced Food Manufacturing Equipment & Technology (FM-2015-05).

References

[1] Davis JR. Metals handbook. second ed. ASM International; 1998.
[2] Liu GZ, Tao NR, Lu K. 316L austenite stainless steels strengthened by means of nano-scale twins. J Mater Sci Technol 2010;26:289–92.
[3] Kashyap BP. Towards interrelationship of grain size, cell parameters and flow stress in type 316L stainless steel. Acta Mater 2002;50:2413–27.
[4] Valiev RZ, Krasilnikov NA, Tsenev NK. Plastic deformation of alloys with submicron-grained structure. Mater Sci Eng, A 1991;137:35–40.
[5] Birringer R, Gleiter H, Klein HP, Marquardt P. Nanocrystalline materials an approach to a novel solid structure with gas-like disorder. Phys Lett A 1984;102:365–9.
[6] Lu K, Wei WD, Wang JT. Grain growth kinetics and interfacial energies in nanocrystalline Ni-P alloys. J Appl Phys 1991;69:7345–7.
[7] Koch CC. The synthesis of non-equilibrium structures by ball-milling. Mater Sci Forum 1992;88–90:243–62.
[8] Tao NR, Wang ZB, Tong WP, Sui ML, Lu J, Lu K. An investigation of surface nanocrystallization mechanism in Fe induced by surface mechanical attrition treatment. Acta Mater 2002;50:4603–16.
[9] Gleiter H. Nanocrystalline materials. Prog Mater Sci 1989;33:223–315.
[10] Chen J, Lu L, Lu K. Hardness and strain rate sensitivity of nanocrystalline Cu. Scripta Mater 2006;54:1913–8.
[11] Lu K, Lu J. Nanostructured surface layer on metallic materials induced by surface mechanical attrition treatment. Mater Sci Eng, A 2004;375–377:38–45.
[12] Lu K, Lu J. Surface nanocrystallization (SNC) of metallic materials – presentation of the concept behind a new approach. J Mater Sci Technol 1999;15:193–7.
[13] Valiev RZ, Korznikov AV, Mulyukov RR. Structure and properties of ultrafine-grained materials produced by severe plastic deformation. Mater Sci Eng, A 1993;168:141–8.
[14] Fang TH, Li WL, Tao NR, Lu K. Revealing extraordinary intrinsic tensile plasticity in gradient nano-grained copper. Science 2011;331:1587–90.
[15] Zhang HW, Hei ZK, Liu G, Lu J, Lu K. Formation of nanostructured surface layer on AISI 304 stainless steel by means of surface mechanical attrition treatment. Acta Mater 2003;51:1871–81.
[16] Lu JZ, Luo KY, Zhang YK, Sun GF, Gu YY, Zhou JZ, Ren XD, Zhang XC, Zhang LF, Chen KM, Cui CY, Jiang YF, Feng AX, Zhang L. Grain refinement mechanism of multiple laser shock processing impacts on ANSI 304 stainless steel. Acta Mater 2010;58:5354–62.
[17] Mordyuk BN, Milman YV, Iefimov MO, Prokopenko GI, Silberschmidt VV, Danylenko MI, Kotko AV. Characterization of ultrasonically peened and laser-shock peened surface layers of AISI 321 stainless steel. Surf Coat Technol 2008;202:4875–83.
[18] Liu S, Gao SY, Zhou YF, Xing XL, Hou XR, Yang YL, Yang QX. A research on the microstructure evolution of austenite stainless steel by surface mechanical attrition treatment. Mater Sci Eng, A 2014;617:127–38.
[19] Chen XH, Lu J, Lu L, Lu K. Tensile properties of a nanocrystalline 316L austenitic stainless steel. Scripta Mater 2005;52:103–1044.
[20] Roland T, Retraint D, Lu K, Lu J. Fatigue life improvement through surface nanostructuring of stainless steel by means of surface mechanical attrition treatment. Scripta Mater 2006;54:1949–54.
[21] Roland T, Retraint D, Lu K, Lu J. Enhanced mechanical behavior of a nanocrystallised stainless steel and its thermal stability. Mater Sci Eng, A 2007;445–446:281–8.
[22] Bai T, Chen P, Guan K. Evaluation of stress corrosion cracking susceptibility of stainless steel 304L with surface nanocrystallization by small punch test. Mater Sci Eng, A 2013;561:498–506.
[23] Chan HL, Ruan HH, Chen AY, Lu J. Optimization of the strain rate to achieve exceptional mechanical properties of 304 stainless steel using high speed ultrasonic surface mechanical attrition treatment. Acta Mater 2010;58:5086–96.
[24] Ye C, Telang A, Gill AS, Suslov S, Idell Y, Zweiacker K, Wiezorek Jörg MK, Zhou Z, Qian D, Mannava SR, Vasudevan VK. Gradient nanostructure and residual stress induced by ultrasonic nano-crystal surface modification in 304 austenitic stainless steel for high strength and high ductility. Mater Sci Eng, A 2014;613:274–88.
[25] Chen AY, Shi SS, Tian HL, Ruan HH, Li X, Pan D, Lu J. Effect of warm deformation on microstructure and mechanical properties of a layered and nanostructured 304 stainless steel. Mater Sci Eng, A 2014;595:34–42.
[26] Balusamy T, Sankara Narayanan TSN, Ravichandran K, Park Il Song, Lee Min Ho. Influence of surface mechanical attrition treatment (SMAT) on the corrosion behaviour of AISI 304 stainless steel. Corros Sci 2013;74:332–44.
[27] Zhang L, Zhang YK, Lu JZ, Dai FZ, Feng AX, Luo KY, Zhong JS, Wang QW, Luo M, Qi H. Effects of laser shock processing on electrochemical corrosion resistance of ANSI 304 stainless steel weldments after cavitation erosion. Corros Sci 2013;66:5–13.
[28] Lu JZ, Qi H, Luo KY, Luo M, Cheng XN. Corrosion behaviour of AISI 304 stainless steel subjected to massive laser shock peening impacts with different pulse energies. Corros Sci 2014;80:53–9.
[29] Lin Y, Lu J, Wang L, Xu T, Xue Q. Surface nanocrystallization by surface mechanical attrition treatment and its effect on structure and properties of plasma nitrided AISI 321 stainless steel. Acta Mater 2006;20:5599–605.
[30] Mordyuk BN, Prokopenko GI, Vasylyev MA, Iefimov MO. Effect of structure evolution induced by ultrasonic peening on the corrosion behavior of AISI-321 stainless steel. Mater Sci Eng, A 2007;458:253–61.
[31] Wang T, Yu J, Dong B. Surface nanocrystallization induced by shot peening and its effect on corrosion resistance of 1Cr18Ni9Ti stainless steel. Surf Coat Technol 2006;200:4777–81.
[32] Chui P, Suna K, Suna C, Yang X, Shan T. Effect of surface nanocrystallization induced by fast multiple rotation rolling on hardness and corrosion behavior of 316L stainless steel. Appl Surf Sci 2011;257:6787–91.
[33] Nikitin I, Altenberger I. Comparison of the fatigue behavior and residual stress stability of laser-shock peened and deep rolled austenitic stainless steel AISI 304 in the temperature range 25–600 °C. Scripta Mater 2004;50:1345–50.
[34] Malaki M, Ding H. A review of ultrasonic peening treatment. Mater Des 2015;87:1072–86.
[35] Sekkal AC, Langlade C, Vannes AB. Tribologically transformed structure of titanium alloy (TiAl6V4) in surface fatigue induced by repeated impacts. Mater Sci Eng, A 2005;393:140–6.
[36] Chen AY, Ruan HH, Wang J, Chan HL, Wang Q, Li Q, Lu J. The influence of strain rate on the microstructure transition of 304 stainless steel. Acta Mater 2011;59:3697–709.
[37] Li J, Chen S, Wu X, Soh A, Lu J. The main factor influencing the tensile properties of surface nano-crystallized graded materials. Mater Sci Eng, A 2010;527:7040–4.
[38] Tian JW, Dai K, Villegas JC, Shaw L, Liaw PK, Klarstrom DL, Ortiz AL. Tensile properties of a nickel-base alloy subjected to surface severe plastic deformation. Mater Sci Eng A 2008;493:176–83.
[39] Tian JW, Shaw L, Liaw PK, Dai K. On the ductility of a surface severely plastically deformed nickel alloy. Mater Sci Eng, A 2008;498:216–24.
[40] Lu L, Chen X, Huang X, Lu K. Revealing the maximum strength in nanotwinned copper. Science 2009;323:607–10.
[41] Meyers MA, Mishra A, Benson DJ. Mechanical properties of nanocrystalline materials. Prog Mater Sci 2006;51:427–556.
[42] Lu JZ, Luo KY, Zhang YK, Zhou JZ, Cui XG, Zhang L, Zhong JW. Effects of laser shock processing and strain rate on tensile property of LY2 aluminum alloy. Mater Sci Eng, A 2010;528:730–5.
[43] Lu L, Schwaiger R, Shan ZW, Dao M, Lu K, Suresh S. Nano-sized twins induce high rate sensitivity of flow stress in pure copper. Acta Mater 2005;53:2169–79.
[44] Wei Q, Cheng S, Ramesh KT, Ma E. Effect of nanocrystalline and ultrafine grain sizes on the strain rate sensitivity and activation volume: fcc versus bcc metals. Mater Sci Eng, A 2004;381:71–9.
[45] Conrad H. Grain size dependence of the plastic deformation kinetics in Cu. Mater Sci Eng, A 2003;341:216–28.
[46] Mao X, Takahashi H. Development of a further miniaturized specimen of 3 mm diameter for TEM disk small punch test. J Nucl Mater 1987;150:42–5.
[47] Li JJ, Soh AK. Modeling of the plastic deformation of nanostructured materials with grain size gradient. Int J Plast 2012;39:88–102.
[48] Moreno-Valle EC, Monclus MA, Molina-Aldareguia JM, Enikeev N, Sabirov I. Biaxial deformation behavior and enhanced formability of ultrafine-grained pure copper. Metall Mater Trans A 2013;44:2399–408.
[49] Liu Y, Jin B, Lu J. Mechanical properties and thermal stability of nanocrystallized pure aluminum produced by surface mechanical attrition treatment. Mater Sci Eng, A 2015;636:446–51.
[50] Zhou F, Lee J, Dallek S, Lavernia EJ. High grain size stability of nanocrystalline Al prepared by mechanical attrition. J Mater Res 2001;16:3451–8.
[51] Sabooni S, Karimzadeh F, Enayati MH. Thermal stability study of ultrafine grained 304L stainless steel produced by martensitic process. J Mater Eng Perform 2014;23:1665–72.
[52] Nikitin I, Altenberger I, Maier HJ, Scholtes B. Mechanical and thermal stability of mechanically induced near-surface nanostructures. Mater Sci Eng, A 2005;403:318–27.